Materials for Quantum Technology

Check for updates

OPEN ACCESS

RECEIVED
13 November 2025

REVISED
28 April 2026

ACCEPTED FOR PUBLICATION
9 June 2026

PUBLISHED
1 July 2026

Original content from this work may be used under the terms of the Creative Commons Attribution 4.0 licence.

Any further distribution of this work must maintain attribution to the author(s) and the title of the work, journal citation and DOI.

PAPER

Telecom wavelength single-photon emission from quasi-resonantly excited InGaSb/AlGaSb quantum dots

Teemu Hakkarainen[1,2,*], **Joonas Hilska**[1], **Arttu Hietalahti**[3], **Sanna Ranta**[1], **Markus Peil**[1], **Robert Matysiak**[4], **Emmi Kantola**[3], **Abhiroop Chellu**[1], **Efsane Sen**[1], **Jussi-Pekka Penttinen**[3], **Anna Musiał**[5], **Michał Gawełczyk**[4] and **Mircea Guina**[1]

[1] Optoelectronics Research Centre, Physics Unit, Tampere University, FI-33720 Tampere, Finland
[2] Institute for Advanced Study, Tampere University, FI-33100 Tampere, Finland
[3] VEXLUM Oy, FI-33710 Tampere, Finland
[4] Institute of Theoretical Physics, Wrocław University of Science and Technology, 50-370 Wrocław, Poland
[5] Department of Experimental Physics, Wrocław University of Science and Technology, 50-370 Wrocław, Poland
[*] Author to whom any correspondence should be addressed.

E-mail: teemu.hakkarainen@tuni.fi

Keywords: quantum dots, single photon, droplet etching, resonant excitation, GaSb materials

Supplementary material for this article is available online

Abstract

Deterministic light sources capable of generating quantum states on-demand at wavelengths compatible with fiber optics and atmospheric transmission windows are essential for practical applications in quantum communication, distributed photonic quantum computing, and quantum metrology. Currently, the technology providing semiconductor quantum emitters with the most promising properties is based on filling droplet-etched nanoholes to form quantum dots (QDs). However, the standard GaAs/AlGaAs material system does not offer telecom window emission. Here, we combine this growth method with antimonide-based materials to demonstrate single-photon emission at 1500 nm from a droplet-etched InGaSb QD. Our device with an antimony-based high refractive index contrast back-reflector designed for cryogenic operation and a solid immersion lens improves photon extraction. QD states are protected by a potential barrier limiting the influx of surrounding carriers, which however prevents revealing excitonic fine structure under nonresonant excitation. In this work, we employ a frequency-tunable continuous wave laser to achieve longitudinal optical (LO) phonon-assisted excitation of the QD ground state and resonant excitation of an excited state. These direct approaches for exciting a single InGaSb QD unlock access to its excitonic fine structure. The typical neutral biexciton–exciton cascade exhibits a negative binding energy of 1.4 meV (2.6 nm) and a fine structure splitting of 24.1 ± 0.4 μeV. Furthermore, we obtain spectrally isolated emission from a charged exciton with a multi-photon probability of 5% with LO phonon-assisted two-color excitation. These results represent a major step towards using this novel antimonide-based QD emitters as deterministic quantum light sources in complex quantum secure networks exploiting the wavelength compatibility with standard telecom fibers.

1. Introduction

Semiconductor light sources capable of generating photonic quantum states on demand are essential building blocks for applications like quantum communication [1–4], quantum computing [5–7] and quantum metrology [8]. In particular, discrete-variable quantum cryptography [9] using light sources emitting single photons [10–12] or pairs of entangled photons [13, 14] enables quantum-secure communication by means of quantum key distribution (QKD). QKD has already been demonstrated at system level in the BB84 scheme using InGaAs/GaAs quantum dots (QDs) [15] emitting at 920 nm and in the Ekert91 scheme using GaAs/AlGaAs QDs emitting polarization-entangled photons at 780 nm

© 2026 The Author(s). Published by IOP Publishing Ltd

[16]. However, these pioneering demonstrations showcasing the capabilities of III–V semiconductor QDs for QKD are either limited to short-range fiber or free-space links [16] or rely on non-linear frequency conversion to shift the emission to a fiber-compatible wavelength [15]. Ultimately, QDs emitting at the wavelengths most compatible with optical fibers and atmospheric transmission windows [17] are essential for practical applications, such as quantum communication networks combining terrestrial optical fibers and satellite links [18, 19]. This need has driven an active exploration and development of alternative QD materials [20, 21] emitting in the 3rd telecom window using various epitaxy approaches including strain-driven Stranski–Krastanov (SK) growth [22] and droplet epitaxy [23] of InAs/InP QDs, and SK growth of InAs QDs on metamorphic layers grown on GaAs [24–26]. State-of-the-art demonstrations with these telecom-range QD systems include reports of multi-photon emission probability as low as $g^{(2)}(0) = (4.4 \pm 0.2) \times 10^{-4}$ [27], high Hong–Ou–Mandel (HOM) visibility of 98% with post-selection [28] and 91.7% without [29], as well as a high-rate intercity BB84 QKD demonstration with 10.9 kbits s^{-1} key rate and quantum bit error ratio of 0.65% [30].

We have recently introduced a new antimonide-based QD system exhibiting narrow-linewidth excitonic emission at 1470 nm [31],formed by GaSb-filling of droplet-etched nanoholes in AlGaSb. GaAs/AlGaAs QDs emitting at 780 nm grown by the same technique exhibit narrow exciton linewidths [32], extremely small inhomogeneous broadening due to size uniformity [33], bright single-photon emission [34], and vanishing fine-structure splitting (FSS) owing to their dimensional symmetry and lack of strain-induced piezoelectric asymmetries[35]. These characteristics have enabled their use as a non-classical light source providing state-of-the-art performance in terms of photon indistinguishability and entanglement [34, 36–38]. The newly developed antimonide-based QDs have already shown several beneficial features, such as extremely homogeneous ensemble emission [31], a suitably low QD density necessary for single-QD devices [31], and single-photon emission in the telecom S-band [39]. However, the advantages of the antimonide material system have not been fully exploited. For example, it offers wide band gap and strain tunability in addition to high refractive index contrast materials for developing efficient photonic structures like Bragg mirrors and waveguides. Moreover, they are compatible with monolithic integration on silicon by direct epitaxial growth because the lattice mismatch between GaSb-based materials and dissimilar substrates can be relaxed right at the first interface by the formation of a network of 90°-dislocations [40, 41] and exploitation of nucleation layers [42]. These unique plastic properties have enabled the epitaxial growth of mid-infrared III-Sb semiconductor lasers on Si substrates [43].

In a recently published work, we identified a 5 meV energy barrier for non-resonantly excited charge carriers to enter the GaSb QD from the surrounding medium [44]. While such a barrier can potentially protect the QD from charge fluctuations when employing coherent resonant excitation [32] or incoherent quasi-resonant excitation [45], it introduces challenges in measuring QD properties when employing above-band excitation. The main challenges include:

- slow emission decay characteristics and volcano-shaped autocorrelation response due to delayed feeding of charge carriers from a reservoir outside the QD [39];
- difficulty in studying the excitonic structure of a single QD due to highly convoluted spectral properties arising from simultaneously exciting a large number of charge complexes and multiple QDs [31, 39];
- Limited achievable photon count rate at excitation powers low enough to produce isolated exciton lines.

These challenges can be overcome by employing quasi-resonant excitation, which allows creation of excitons directly in the QD. If the excitation is tuned in resonance with *p*-shell transitions [45, 46] or transitions involving other excited states (ES), it is followed by phonon-mediated relaxation of carriers into the ground state and subsequent radiative recombination of the exciton. The required relaxation processes can cause considerable contribution to the system dynamics, particularly, if the required energy loss in the relaxation process is smaller than the optical phonon energy but too high for efficient acoustic-phonon emission, causing the so-called phonon bottleneck [45]. Alternatively, the QD can be excited quasi-resonantly through phonon-assisted absorption processes involving either acoustic [45, 47–49] or optical phonons [45]. A typical laser detuning for a longitudinal acoustic (LA) phonon-assisted excitation is in the range of few meV or less [47, 48], while longitudinal optical (LO) phonon-assisted excitation requires a detuning of tens of meV to match the LO phonon energy of the material [45]. Consequently, LO phonon-assisted excitation allows use of low-cost long-pass filters to separate

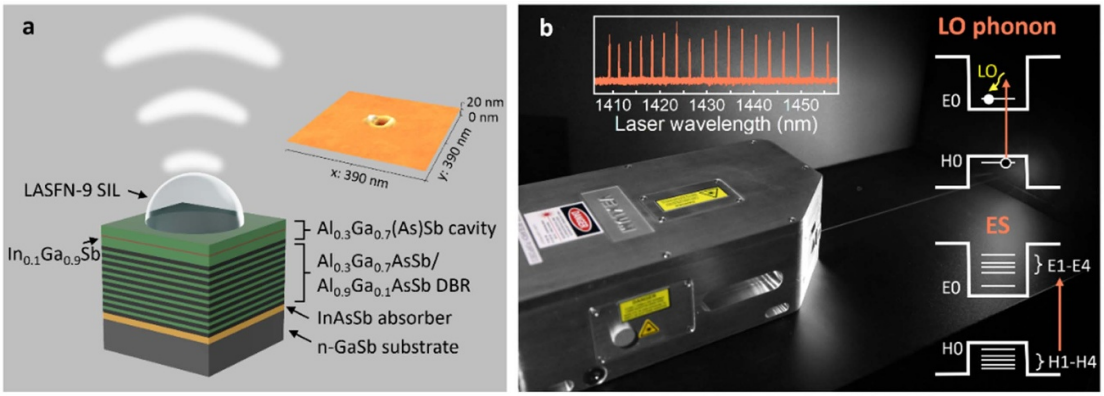

Figure 1. (a) Schematic illustration of the antimonide-based QD device. The QDs, located in the middle of the AlGa(As)Sb λ-cavity, were grown by filling droplet-etched nanoholes with $In_{0.1}Ga_{0.9}Sb$. The surface profile of a nanohole is shown in the inset. The bottom mirror is a 9.5-pair AlGaAsSb distributed Bragg reflector (DBR). The device structure is separated from the substrate with an InAsSb absorber to block unwanted luminescence from the n-GaSb at the QD emission wavelength. A hemispherical solid immersion lens (SILs) is bonded on top of the semiconductor structure to enhance photon extraction. (b) The QD device is excited with a vertical external cavity surface emitting laser (VECSEL) providing single-frequency continuous-wave operation from 1400 to 1470 nm. These wavelengths allow LO phonon-assisted excitation of the QD ground state (H0–E0) and quasi-resonant excitation of transitions involving excited states (ES) of holes (H1–H4) and electrons (E1–E4).

the laser photons from the QD emission, while more sophisticated filtering methods are required for LA phonon-assisted excitation. In the case of GaAs/AlGaAs QDs, it has been demonstrated that LO phonon-assisted excitation produces similar luminescence lifetime, $g^{(2)}(0)$, and HOM visibility as strictly resonance fluorescence, and spectral purity similar to LA phonon-assisted excitation [45]. Thus, LO phonon-assisted excitation is an effective quasi-resonant excitation method in terms of suppression of unwanted re-excitation and robustness against spectral diffusion and charge noise similar to more commonly used LA phonon-assisted excitation [47, 48].

In this work, we introduce a single-photon emitter based on a single InGaSb/AlGaSb QD (figure 1(a)) with an indium content of 10% corresponding to emission at 1500 nm wavelength region. A compact frequency-tunable single-frequency semiconductor laser operating in continuous-wave regime in the 1400–1470 nm range (figure 1(b), supplementary material section 3) is used as the excitation source. This laser enables quasi-resonant pumping of the QD via its and ground state via LO phonon-mediated pathways. Consequently, we gain access to the excitonic fine-structure of InGaSb/AlGaSb QDs and their single-photon emission characteristics without the convoluted dynamics caused by the charge reservoir.

2. Experimental details

2.1. Sample fabrication

The epitaxial heterostructure shown in figure 1 was grown by molecular beam epitaxy (MBE). The layer sequence starts with a 400 nm thick lattice-matched InAsSb layer, which acts as an absorber to minimize unwanted photoluminescence (PL) emission from the n-GaSb(100) substrate. The absorber is then capped with a protective 2 nm GaSb layer after which a 9.5-pair bottom Bragg reflector mirror is grown with lattice-matched $Al_{0.9}Ga_{0.1}As_{0.07}Sb_{0.93}/Al_{0.3}Ga_{0.7}As_{0.03}Sb_{0.97}$ pairs. Finally, a 1λ-thick $Al_{0.3}Ga_{0.7}Sb$ microcavity is grown consisting of two outer ¼λ-thick $Al_{0.3}Ga_{0.7}As_{0.03}Sb_{0.97}$ and two inner ¼λ-thick As-free $Al_{0.3}Ga_{0.7}Sb$ pairs. The QDs are placed at the center of the cavity and are formed by Al-droplet mediated nanohole etching on the $Al_{0.3}Ga_{0.7}Sb$ surface and subsequent filling of the nanoholes by 7.2 monolayers (MLs) of $In_{0.1}Ga_{0.9}Sb$. The etching parameters follow those found in our earlier reports [31, 39]. Namely, the droplets are etched at a temperature of 395 °C under a low Sb-flux of ~0.06 ML s^{-1} for 180 s. The geometry of the resulting nanoholes is shown in figure S1 in the supplementary material.

A hemispherical LASFN-9 SILs was attached on top of the MBE-grown sample. The combination of a distributed Bragg reflector (DBR) back-reflector and SIL improves the photon collection efficiency but does not provide Purcell enhancement. The results of numerical finite difference time domain (FDTD) simulation of the collection efficiency and the far-field patterns of the QD emission are presented in

section 2 of the supplementary material. According to the FDTD simulations, introduction of DBR and SIL improves the photon extraction efficiency in a numerical aperture (NA) of 0.81 from 1.2% to 16%.

2.2. Optical experiments

The optical experiments were carried out with a setup custom-built around a low-vibration pulse-tube cryostat cooled down to 5 K. A schematic of the complete setup is presented in figure S5 in the supplementary material. The sample was excited with the semiconductor laser described in section 2.3. An additional 950 nm LED was used as an optional above-band excitation source for two-color excitation. The power density of the LED was estimated as 200 W m^{-2} at the back aperture of the objective and the area of the field of view. The LED intensity was optimized for charged trion (X^*) emission intensity and kept at a level that would not produce detectable QD emission without the laser. The excitation beams were combined with non-polarizing beam splitters and focused on the sample with a 60-times magnifying NA = 0.81 objective located inside the cryostat. The laser spot size was around 1–2 μm. The same objective was used to collect the emitted photons. A 1470 nm long-pass filter was used to block the back-scattered laser beam during luminescence measurements. The polarization of the laser was controlled with a rotatable $\lambda/2$ waveplate. In polarization-dependent measurements of the QD emission, the detection polarization was filtered using a rotatable $\lambda/2$ waveplate and a fixed polarizer. The laser power was controlled with a variable neutral density filter. The rotation of the neutral density filter, waveplates, and the laser birefringent filter (BRF) was automated and integrated as a part of the spectral acquisition software.

The luminescence signal was dispersed on a thermoelectric-cooled InGaAs array with a 750 mm spectrograph equipped with a 600 l mm^{-1} grating. The resulting spectral resolution of the setup was 80 μeV. The single-photon counting was carried out using the secondary output port of the spectrometer. The photons corresponding to a single emission line were coupled into a 100 m long single-mode fiber to transfer them to another laboratory where the single-photon detection setup is located. The antibunching experiment was carried out at the other end of the fiber using a Hanbury–Brown–Twiss configuration consisting of a 50/50 fiber beam splitter and a pair of superconducting nanowire single-photon detectors. The photon statistics were counted using 39 ps bin size. The combined timing resolution of the detectors and the timing electronics is 40 ps.

2.3. Excitation laser

The excitation laser used in this work is an optically pumped vertical-external-cavity surface-emitting laser (OP-VECSEL [50]). VECSELs combine the advantages of external-cavity solid-state disk lasers with those of quantum well (QW) semiconductor lasers and provide high output power, excellent beam quality, low noise, high spectral purity, and tunable wavelength versatile operation in a compact footprint. Although still perceived as an emerging laser technology, VECSELs have made considerable progress over the last decade [51, 52] and are becoming key building blocks for atomic, molecular and optical physics experiments.

The VECSEL used in this work is a first-of-a-kind prototype of a VALO SF system from Vexlum Inc for QD excitation. The VALO SF laser platform has been particularly developed for atom and ion-based quantum systems [51, 52], offering low-noise operation down to sub-Hz linewidths [53], wavelength flexibility, high beam quality, and accurate frequency tuning for tens of nm over longitudinal modes and GHz-level of hop-free tuning range, which is sufficient for scanning across the absorption line of a transform limited QD. The laser includes the VECSEL head, control electronics, and a low-noise chiller. The VECSEL head comprises a semiconductor gain mirror with AlGaInAs QW with PL centered at 1428 nm at room temperature, an external cavity with 1% output-coupling mirror mounted on a piezo actuator and with $\sim$1 GHz free-spectral range (FSR), and a fiber-coupled 808 nm diode pump laser for carrier excitation. In a free-running configuration (i.e., with an empty cavity), the laser outputs $>$3.5 W of output power at around 1460 nm. To allow broadly tunable single-frequency operation between 1400 and 1470 nm, a 3 mm thick BRF is placed inside the laser cavity and further mounted on a rotation mount with resonant piezoelectric motors to enable precise remote control of the BRF rotation angle around its optical axis and thus the laser wavelength. During BRF rotation, a 6 kHz square wave with a 15 V amplitude is applied to the output coupler piezo to force the laser to jump through all cavity modes with 1 GHz resolution originating from the cavity FSR, which is fine enough to access all absorption lines of a QD. This driving allows fast hopping between cavity modes without skipping. The resulting wavelength tuning range is shown in figure S4(a).

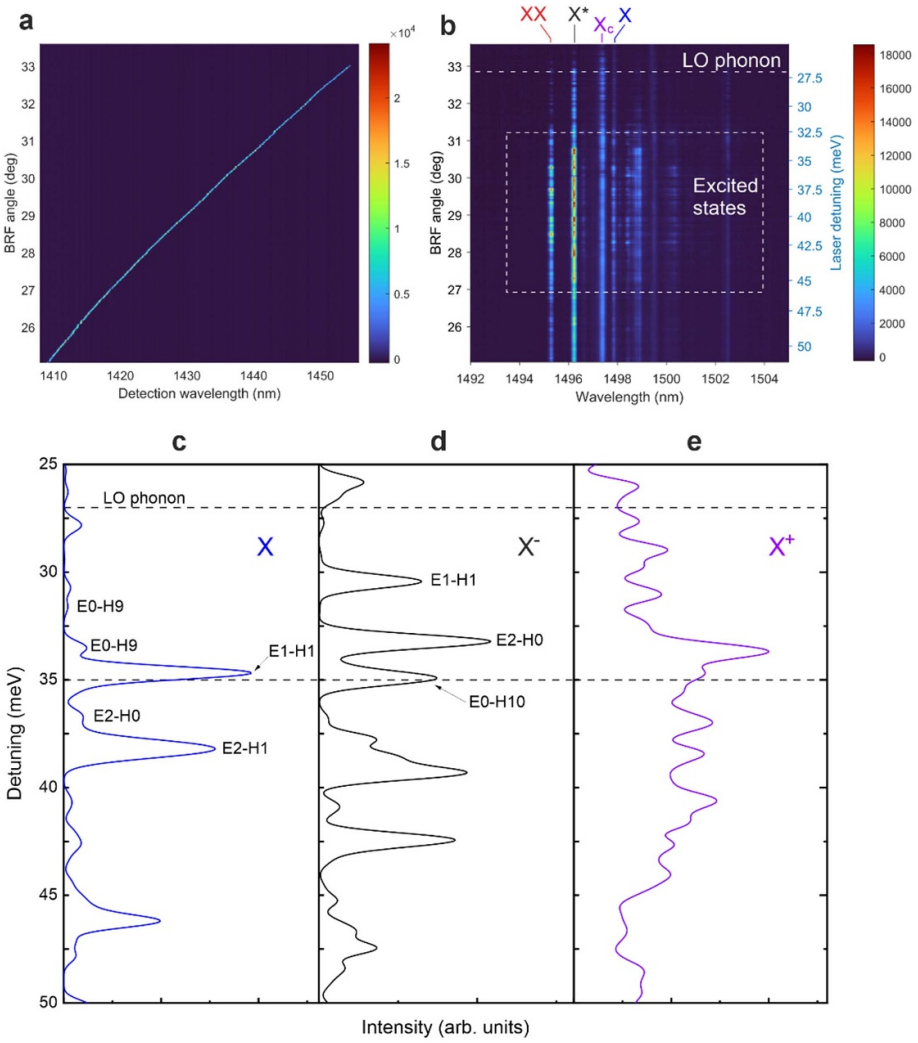

Figure 2. (a) Single-mode lasing characteristic of the frequency-tunable excitation laser. The laser spectrum was detected from the intensity reflected from the QD device. The laser wavelength is tuned by rotating a BRF inside the laser cavity. (b) PLE results for a single InGaSb QD obtained with a laser excitation power of 4 μW maintained across different excitation wavelengths. Absorption spectra obtained from numerical simulations for (c) neutral exciton, (d) negative trion, and (e) positive trion. The dashed lines in (c)–(e) indicate the laser detunings used in the experiments for LO phonon-assisted excitation and ES excitation.

3. Results

The optical experiments were carried out for InGaSb QDs embedded in the device structure presented in figure 1(a). The device combines a Bragg mirror back-reflector and a SIL for improving the photon collection efficiency into the available microscope objective. As explained in the supplementary material section 2, which deals with the optical design of the device, we expect around 16% collection efficiency for NA = 0.81. First, we scan the BRF of the laser to sweep the lasing wavelength across the tuning range and record the back-reflected laser intensity as a function of wavelength. As shown in figure 2(a), single-mode output is observed throughout the tuning range.

3.1. Photoluminescence excitation spectroscopy (PLE)

To identify absorption bands enabling quasi-resonant excitation of a single QD, we use PLE, where the QD emission spectrum in the 1500 nm range is recorded as a function of excitation wavelength. As shown in figure 2(b), the intensity of the excitonic emission lines of the QD varies as a function of the excitation wavelength. Based on the PL spectrum of a QD ensemble (see figure S2 in the supplementary material), we expect the transition involving the first excited electron and hole states (E2–H2) to be at 1430 nm, which is at a separation of approximately 38 meV from the ground state transition energy. Since absorption can occur through transitions not visible in the PL spectrum, we use simulations performed within the combined framework of 8-band $k\cdot p$ and configuration-interaction methods

(supplementary material section 8) to identify the peaks in figure 2(b) arising from transitions predominantly involving different electron and hole states. Figure 2(c) shows the simulated absorption spectrum, with the intensity of lines obtained from the transition oscillator strengths and their broadening accounting for both the natural Fourier-limited linewidth and an additional inhomogeneous broadening of 0.35 meV. The most pronounced peaks are related to transitions involving the lowest two hole states (H1 and H2) and the first excited electron states (E2 and E3). At the higher end of the laser tuning range, we observe a narrow resonance of the most pronounced emission line (X^*) peaking at a detuning of 27 meV. This line arises from the excitation of the 1496.3 nm emission assisted by emission of a single LO phonon [45, 54] (GaSb-like LO phonon in the $Al_{0.3}Ga_{0.7}Sb$ barrier [55]). In the following experiments, we excite the QD by targeting either the E1–H1 (neutral exciton) and E0H10 (negative trion) transitions at a detuning of 35 meV (BRF 30.4°) or the ground state E0–H0 through LO phonon-assisted excitation at a detuning of 27 meV (BRF 32.8°). From now on, we refer to optical pumping of carriers to the quasi-resonant E1–H1 and E0H10 transition as ES excitation.

3.2. Excited state excitation

In order to investigate the excitonic structure of the QD emission, we record the emitted PL spectrum as a function of detection polarization using ES excitation (figure 3). As shown in figure 3(a), two emission lines exhibit fine structure evidenced by their polarization-dependent peak position. These lines are identified as a neutral exciton (X) at 1498.0 nm and biexciton (XX) at 1495.4 nm from power-dependent PL data (supplementary material section 7). The dominant emission line at 1496.3 nm showing no fine structure is identified as a trion (X^*). Given the p-type nature of native defects in antimonide materials [56, 57], X^* could be assigned as a positively charged trion based on the expected charge carrier statistics in the AlGaSb barrier and the intensity of the peak. However, the PLE response of the X^* line (figure 3(b)) does not agree with the simulated absorption spectrum of positively charged trion (figure 3(e)) which is characterized by a large number of overlapping absorption peaks resulting in a quasi-continuous absorption band due to low separation of hole states. On the other hand, the simulated absorption spectrum of a negatively charged trion matches well with the PLE response of the X^* line. Thus, we assign X^* line as a negatively charged trion. We attribute the predominant negative charging of the QD to trapping of photo-generated charge being in favor of lighter electrons over heavier holes due to the 5 meV energy barrier for charge transfer from QW to QD [44]. The weak periodic modulation of the X^* line intensity with the polarization angle can be translated into a degree of linear polarization of 0.14 and further to a 1.5% opposite-spin light hole admixture to the hole ground state [58]. The exciton line located between X and X^* is then the positively charged trion, which shows no fine structure and has a power-dependency similar to the negatively charged X^*. This line is referred to as X_c in the supplementary material. We note also that the PLE response of the X_c line is in agreement with the simulated absorption spectrum of a positively charged trion (figure (e)) resembling a quasi-continuous absorption band. The exciton peak assignment is supported by the excitation power dependent data shown in figure S8 in the supplementary material, where we observe a competition between the differently charged trions when the excitation power is changed. The positive charging due to the p-type carrier concentration of the barrier material dominates at low excitation powers, while a shift in favor of negative charging is observed when the concentration of photo-generated excess charge increases with increasing laser power. Noticeably, the dynamics can be shifted more in favor of the dominant negatively charged X^* at 1496.3 nm by adding a 950 nm LED as a weak above-band excitation source (from now onwards referred to as two-color excitation[59]).

Now that we have provided an overview of the PL spectrum of a single InGaSb/AlGaSb QD and identified the different charge complexes, we can proceed to analyze the excitonic structure in more detail. A neutral biexciton binding energy, $\Delta E_{XX} = E_X - E_{XX} = -1.4$ meV (-2.6 nm), is obtained from the X–XX peak separation. Similar behavior is observed for another QD as shown in figure S7(a) in the supplementary material. The absolute values of ΔE_{XX} observed here are comparable to those seen in droplet-etched GaAs/AlGaAs QDs [33, 34, 36, 60], which, however, tend to have positive values. For the InGaSb/AlGaSb QDs investigated here, the observed negative values of ΔE_{XX} despite quite large confinement volume suggests some spatial separation of electrons and holes in a QD [61].

An FSS of 24.1 $\pm$ 0.4 μeV is obtained from a sinusoidal fit to the XX peak position. Based on the investigation of 5 QDs, we conclude that this is a typical value for the investigated sample since we mainly observe FSS values in the 20–26 μeV range (figure S7 in the supplementary material), while an outlier with FSS = 5.1 $\pm$ 0.3 μeV is also identified. Overall, the observed FSS values indicate that further growth optimization for improving the QD symmetry is required to reduce the FSS to a level required for high fidelity of polarization entanglement. All investigated QDs have emission polarized in the same direction (figure S7c), which suggests that the FSS is mainly due to the QD shape asymmetry. As shown

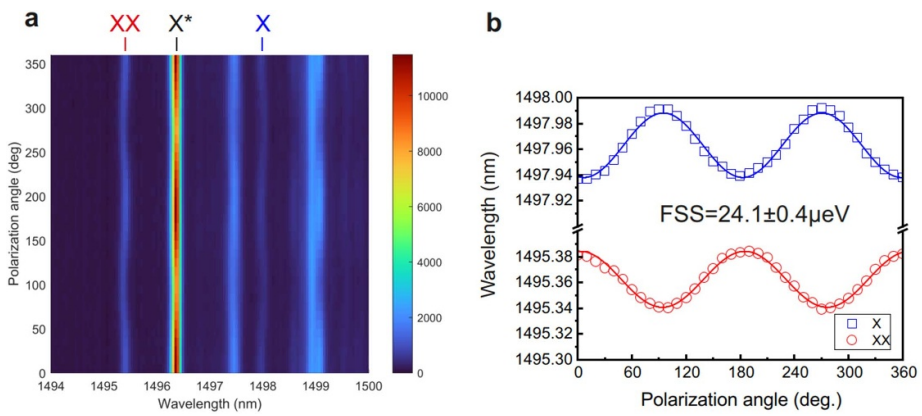

Figure 3. (a) Polarization-resolved emission spectrum of a single QD with ES excitation. The *X* and *XX* emission lines exhibit FSS, with their emission wavelength varying periodically as a function of polarization, while the X^* line is polarization-independent. (b) FSS evaluated from a sinusoidal fit to the peak wavelength values obtained from a Gaussian fit.

in figure S1, the lower part of the nanohole is highly symmetric while a clear asymmetry is observed towards the upper part near the ring structure around the nanohole. A possible route to reduce the FSS could be to reduce the in-filling amount and form a structure where the quantum confinement is predominantly defined by the symmetric lower part of the nanohole or symmetrizing the upper part of the nanohole and the surrounding ring structure. Reducing the intrinsic FSS values to 6–8 μeV in this manner would then make it possible to tune it down to zero by either strain-tuning [62] or AC stark tuning [63].

3.3. LO phonon-assisted excitation

As shown in figure 3 and discussed above, the ES excitation scheme is effective for revealing the full excitonic structure and for investigating the fine structure of the confined states in the QD. It has been demonstrated for GaAs/AlGaAs QDs that it is possible to achieve similar $g^{(2)}(0)$ and HOM visibility using LO phonon-assisted excitation and strictly resonant fluorescence [45]. Therefore, we set the laser wavelength to 1449 nm for LO phonon-assisted excitation of the QD ground state. As shown in figure 4(a), this results in an emission spectrum dominated by the X^* transition. By implementing two-color excitation [59] (i.e. using a 950 nm LED for above-band excitation of the AlGaSb barrier in addition to the laser used for LO phonon-assisted excitation), we can further shift the charge dynamics in favor of X^*, with 60% of the spectrally integrated intensity now being emitted from the X^* transition. The exciton linewidth is noted to be limited by the spectral resolution of the setup (80 μeV) both with and without two-color excitation.

Figure 4(b) shows a second-order autocorrelation trace of the X^* emission line counted in a fiber-based Hanbury–Brown–Twiss configuration (40 ps timing resolution) using the two-color excitation scheme. The experimental data is fitted with a model that includes photon antibunching (single-photon emission) and spectral blinking [64]. The model parameters include the multi-photon emission probability $g^{(2)}(0)$, the emission on-time β related to blinking process, as well as the blinking time constant τ_{Blink} and the correlation time τ_{Corr}, which includes the radiative lifetime of the exciton, and in case of incoherent excitation, additional contributions from relaxation and capture dynamics. From the fit we obtain a $g^{(2)}(0) = 0.05 \pm 0.03$, which compares well with the value of 0.019 ± 0.001 reported for GaAs/AlGaAs QDs under similar experimental conditions (LO phonon-assisted excitation) [45] but does not reach the record values of telecom QDs [27, 28]. We expect to observe much lower values of $g^{(2)}(0)$ in the future for our InGaSb/AlGaSb QDs by (i) subduing emission from the GaSb substrate which currently contributes detrimentally to the autocorrelation experiments and (ii) improving the low count rate due to the inefficient fiber coupling which ultimately affects the $g^{(2)}(0)$ fitting process.

The observed blinking characteristics are similar to the values reported in GaAs/AlGaAs QDs without applying an electric field bias to stabilize the charge environment. The emission on-time, $\beta = 0.35 \pm 0.007$, is similar to what is seen in GaAs/AlGaAs QDs under resonant excitation [65] and reasonably better than GaAs/AlGaAs QDs under quasi-resonant excitation [64], while $\tau_{\mathrm{Blink}} = 26.2 \pm 1.1$ ns is also similar to the GaAs/AlGaAs QDs [64]. Figure 4(c) shows the second-order autocorrelation trace of the X^* emission line under ES excitation. The result from the fit is quite similar to the LO phonon-assisted excitation for τ_{Blink}, but a slightly larger emission on-time with

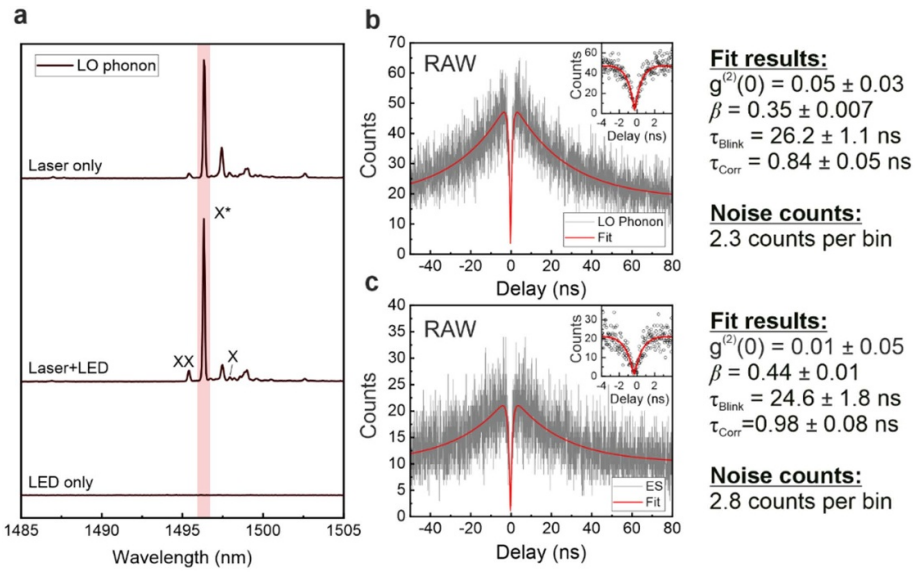

Figure 4. (a) Single-QD emission spectrum obtained with 4.5 μW LO phonon-assisted excitation. The plot shows the spectrum for excitation with laser only and for two-color excitation, where a 950 nm LED was added for tuning the charge distribution in the AlGaSb barrier. The LED power density was set to 200 W m^{-2}, which was low enough not to produce detectable emission when the laser was switched off. (b) Second-order autocorrelation trace of the X^* line with LO phonon-assisted two-color excitation [59]. (c) Second-order autocorrelation trace of the X^* line with ES excitation. A two-level model was fitted to the autocorrelation traces to obtain the physical parameters of quantifying photon antibunching and spectral blinking [64]. The insets in (b) and (c) show a zoomed-in view of the zero-delay region.

$\beta = 0.44 \pm 0.01$ and $g^{(2)}(0) = 0.01 \pm 0.05$ are revealed. It should be noted that while the autocorrelation characteristics are quite similar for the two excitation methods, LO phonon-assisted excitation provides a higher count rate thanks to the emission predominantly by X^* recombination. This is particularly so when the two-color excitation is applied.

The correlation time τ_{Corr} defines the width of the antibunching dip at zero-delay. In the simplest case of a two-level system, it would be determined by the spontaneous radiative lifetime of the emitter. However, in the case of quasi-resonant excitation, the value of τ_{Corr} may additionally include the component of temporal delay arising from the thermalization process involved in the spontaneous radiative decay from the X^* state. This is particularly the case for the ES excitation, which is better described as a three-level system. For LO phonon-assisted excitation, we get $\tau_{\mathrm{Corr}} = 0.84 \pm 0.05$ ns, while for ES excitation, it is slightly slower with $\tau_{\mathrm{Corr}} = 0.98 \pm 0.08$ ns. These values are somewhat larger than 0.32 ns reported for weakly confined GaAs/AlGaAs QDs [64], but of a similar magnitude to typical radiative lifetimes of radiatively efficient systems like In(Ga)As/GaAs QDs emitting at 920 nm [66] and InAs/InGaAs QDs emitting at 1550 nm [26]. The true radiative lifetimes of the InGaSb/AlGaSb QDs will be assessed in our future work using a pulsed semiconductor laser, which is currently under development.

4. Discussion

We have introduced InGaSb/AlGaSb QDs formed by filling droplet-etched nanoholes as a new single-photon source emitting in the 1500 nm wavelength range. A compact frequency-tunable semiconductor laser is utilized for PLE spectroscopy, which is carried out within the excitation wavelength range, covering both quasi-resonant ES excitation and LO phonon-assisted excitation of the QD ground state. By exciting the QD states directly, we can eliminate the complex charge dynamics arising from delayed feeding of charge carriers from a reservoir outside the QD, which are present when using above-band excitation. Consequently, we achieve spectrally pure emission predominantly from a single charged exciton line (X^*) and pure single-photon emission with $g^{(2)}(0) = 0.05 \pm 0.03$. This is a considerable improvement compared to our previous work with above-band excitation, resulting in non-ideal spectral features and $g^{(2)}(0) = 0.16 \pm 0.02$ [39]. These results compare well with the data collected from GaAs/AlGaAs QDs under similar experimental conditions in terms of single-photon purity, spectral features, and blinking characteristics [45, 64]. The InGaSb/AlGaSb QDs are thus expected to respond well to the application of

an electric field bias from a p–i–n diode for charge stabilization, which is known to completely eliminate blinking in GaAs/AlGaAs QDs [32, 65].

Furthermore, exciting the QD states directly enabled us to obtain a detailed overview of the excitonic structure. Additionally, this allowed for measuring the key physical properties relevant to further developing antimonide QDs for high-quality single- and entangled-photon emission in the third telecom window. In particular, the biexciton binding energy $\Delta E_{XX} = -1.4$ meV (-2.6 nm) is large enough to render possible coherent pumping of the biexciton–exciton cascade by two-photon absorption [32, 65]. Moreover, the FSS values obtained from the investigated QDs ranges from 5 to 26 μeV (figures 3, figure S7), with the larger end of the range being more representative of the population. While these values are not small enough for the generation of polarization-entangled photons with high fidelity, they are a good starting point for optimization. Since the nanoholes etched in AlGaSb with Al droplets are highly symmetric (figure S1 in the supplementary material), the FSS can result from asymmetric filling, piezoelectric asymmetry resulting from the 0.63% lattice-mismatch between the $In_{0.1}Ga_{0.9}Sb$ QD material and the GaSb substrate, atomistic details of QD material alloying, or heavy-light hole mixing enhanced due to low biaxial strain even in an almost symmetric QD. It should be noted, however, that the expected lattice strain is an order of magnitude smaller than, for example, in the InAs/GaAs system (7%). Nevertheless, there is viability for reducing the indium content and simultaneously increasing the QD size to reduce the alloying and piezoelectric effects and increasing the heavy-light hole splitting, while still maintaining emission in the 1500 nm wavelength region. Such a change in the QD structure would shift the resulting energy structure towards even weaker confinement and provide certain benefits such as positive biexciton binding energy and a faster radiative rate as seen in GaAs/AlGaAs QDs [45]. It has been recently shown that high-indium-content $In_xGa_{1-x}As$/AlGaAs QDs (with $x = 0.1$–0.4) grown in droplet-etched nanoholes can exhibit as low FSS as pure GaAs QDs with no clear correlation between FSS and indium content [67]. Therefore, it is more likely that cause for the FSS observed in our $In_{0.1}Ga_{0.9}Sb$/AlGaSb is related to QD shape asymmetry. To this end, symmetrizing the upper part of the nanohole and the surrounding ring structure by careful adjustment of the epitaxial growth has played an important role in minimizing the FSS in GaAs/AlGaAs QDs [68]. This approach can be adopted to the InGaSb/AlGaSb QDs.

5. Conclusion

In summary, we revealed the fundamental optical properties of InGaSb/AlGaSb QDs formed by filling droplet-etched nanoholes. The QDs are embedded in a device structure comprising an antimonide-based Bragg reflector and a SIL to improve photon collection. Exciting the InGaSb/AlGaSb QDs quasi-resonantly with a compact frequency-tunable semiconductor laser allowed us to study their excitonic fine structure with unprecedented detail. Furthermore, directly addressing the energy states of single QDs allowed us to achieve predominant emission from a single exciton line with a low multi-photon emission probability of $g^{(2)}(0) = 0.05 \pm 0.03$. These results represent a major step towards developing antimonide-based QD materials for quantum photonics and applying a wavelength-flexible semiconductor laser platform as an excitation source for deterministic quantum emitters in secure fiber-based quantum networks.

Acknowledgments

Financial support from the Finnish Research Council projects QuantSi (Decision No. 323989) and CryoLight (Decision No. 357351), Business Finland co-innovation project QuTI (41739/31/2020), Business Finland Rise to Challenge project TeleQuant (1835/31/2025), the Research Council of Finland Flagship Programm PREIN, and FiGAnti project funded within the QuantERA II Programme that has received funding from the European Union's Horizon 2020 research and innovation program under Grant Agreement No. 101017733 and National Science Centre, Poland—Project 2023/05/Y/ST3/00125 is acknowledged. TH acknowledges financial support from Tampere University Institute of Advanced Study. M. G. and R. M. are grateful to Krzysztof Gawarecki for sharing his computational code. The authors would like to thank Professor Robert Fickler, Lea Kopf, and Jaime Moreno Zuleta for their help in the single-photon autocorrelation experiments.

Data availability statement

All data that support the findings of this study are included within the article (and any supplementary files).

Supplementary data 1 available at https://doi.org/10.1088/2633-4356/ae7ad9/data1.

Conflict of interest

Authors declare no conflicts of interest.

Funding

Finnish Research Council project QuantSi (Decision No. 323989); Finnish Research Council project CryoLight (Decision No. 357351); Business Finland co-innovation project QuTI (41739/31/2020); FiGAnti project (Grant Agreement No. 101017733) funded within the QuantERA II Programme; Business Finland Rise to Challenge project TeleQuant (1835/31/2025); National Science Centre, Poland—project 2023/05/Y/ST3/00125.

Author contributions

Teemu Hakkarainen 0000-0001-6758-2496
Conceptualization (lead), Data curation (lead), Formal analysis (lead), Funding acquisition (supporting), Investigation (lead), Methodology (lead), Supervision (supporting), Writing – original draft (lead)

Joonas Hilska 0000-0002-0595-8993
Conceptualization (supporting), Data curation (supporting), Formal analysis (supporting), Investigation (supporting), Methodology (supporting), Writing – original draft (supporting)

Arttu Hietalahti
Data curation (supporting), Methodology (supporting), Writing – original draft (supporting)

Sanna Ranta
Data curation (supporting), Investigation (supporting), Methodology (supporting)

Markus Peil
Data curation (supporting), Investigation (supporting)

Robert Matysiak
Data curation (supporting), Investigation (supporting), Writing – review & editing (supporting)

Emmi Kantola
Conceptualization (supporting)

Abhiroop Chellu 0000-0001-5965-4234
Data curation (supporting), Writing – original draft (supporting)

Efsane Sen
Data curation (supporting)

Jussi-Pekka Penttinen
Conceptualization (supporting), Funding acquisition (supporting), Supervision (supporting), Writing – original draft (supporting)

Anna Musiał 0000-0001-9602-8929
Conceptualization (supporting), Funding acquisition (supporting), Supervision (supporting), Writing – original draft (supporting)

Michał Gawełczyk 0000-0003-2299-140X
Data curation (supporting), Formal analysis (supporting), Supervision (supporting), Writing – original draft (supporting)

Mircea Guina
Funding acquisition (lead), Supervision (lead)

References

[1] Yamamoto Y 2006 Quantum communication and information processing with quantum dots *Quantum Inf. Process.* **5** 299–311
[2] Bouwmeester D, Ekert A and Zeiliger A 2013 *The Physics of Quantum Information* (Springer) (https://doi.org/10.1007/978-3-662-04209-0)
[3] Vajner D A, Rickert L, Gao T, Kaymazlar K and Heindel T 2022 Quantum communication using semiconductor quantum dots *Adv. Quantum Technol.* **5** 2100116
[4] Heindel T *et al* 2023 Quantum dots for photonic quantum information technology *Adv. Opt. Photon.* **15** 613
[5] Knill E, Laflamme R and Milburng G J 2001 A scheme for efficient quantum computation with linear optics *Nature* **409** 46–52
[6] Wang H *et al* 2019 Boson sampling with 20 input photons and a 60-mode interferometer in a 1014-dimensional Hilbert space *Phys. Rev. Lett.* **123** 250503
[7] Zhong H-S *et al* 2020 Quantum computational advantage using photons *Science* **370** 1460–3
[8] Peniakov G, Su Z-E, Beck A, Cogan D, Amar O and Gershoni D 2020 Towards supersensitive optical phase measurement using a deterministic source of entangled multiphoton states *Phys. Rev. B* **101** 245406
[9] Gisin N, Ribordy G, Tittel W and Zbinden H 2022 Quantum cryptography *Rev. Mod. Phys.* **74** 145
[10] Intallura P M, Ward M B, Karimov O Z, Yuan Z L, See P, Shields A J, Atkinson P and Ritchie D A 2007 Quantum key distribution using a triggered quantum dot source emitting near 1.3 μm *Appl. Phys. Lett.* **91** 161103
[11] Rau M *et al* 2014 Free space quantum key distribution over 500 meters using electrically driven quantum dot single-photon sources—a proof of principle experiment *New J. Phys.* **16** 043003
[12] Bozzio M, Vyvlecka M, Cosacchi M, Nawrath C, Seidelmann T, Loredo J C, Portalupi S L, Axt V M, Michler P and Walther P 2022 Enhancing quantum cryptography with quantum dot single-photon sources *npj Quantum Inf.* **8** 104
[13] Yuan Z-S, Bao X-H, Lu C-Y, Zhang J, Peng C-Z and Pan J-W 2010 Entangled photons and quantum communication *Phys. Rep.* **497** 1–40
[14] Schimpf C, Reindl M, Huber D, Lehner B, Covre Da Silva S F, Manna S, Vyvlecka M, Walther P and Rastelli A 2021 Quantum cryptography with highly entangled photons from semiconductor quantum dots *Sci. Adv.* **7** eabe8905
[15] Zahidy M *et al* 2024 Quantum key distribution using deterministic single-photon sources over a field-installed fibre link *npj Quantum Inf.* **10** 2
[16] Basset F B *et al* 2021 Quantum key distribution with entangled photons generated on demand by a quantum dot *Sci. Adv.* **7** 6379
[17] Yin J *et al* 2017 Satellite-based entanglement distribution over 1200 kilometers *Science* **356** 1140–4
[18] Bakker D L, Jong Y, Dirks B P F and Amaral G C 2024 A best-path approach to the design of a hybrid space-ground quantum network with dynamic constraints *Photonics* **11** 268
[19] Li Y *et al* 2025 Microsatellite-based real-time quantum key distribution *Nature* **640** 47–54
[20] Ying Y, Liu S, Lee C-M, Michler P, Reitzenstein S, Srinivasan K, Waks E and Liu J 2023 Telecom-band quantum dot technologies for long-distance quantum networks *Nat. Nanotechnol.* **18** 1389
[21] Thapa D K and Biswas S 2025 Single photon generation from quantum dots: recent advances, challenges and future directions *Nanoscale* **17** 7651–72
[22] Musiał A, Mikulicz M, Mrowiński P, Zielińska A, Sitarek P, Wyborski P, Kuniej M, Reithmaier J P, Sęk G and Benyoucef M 2021 InP-based single-photon sources operating at telecom C-band with increased extraction efficiency *Appl. Phys. Lett.* **118** 221101
[23] Müller T, Skiba-szymanska J, Krysa A B, Huwer J, Felle M, Anderson M, Stevenson R M, Heffernan J, Ritchie D A and Shields A J 2018 A quantum light-emitting diode for the standard telecom window around 1550 nm *Nat. Commun.* **9** 862
[24] Zeuner K D *et al* 2021 On-demand generation of entangled photon pairs in the telecom C-band with InAs quantum dots *ACS Photonics* **8** 2337
[25] Deutsch D, Buchholz C, Zolatanosha V, Jöns K D and Reuter D 2023 elecom C-band photon emission from (In,Ga)As quantum dots generated by filling nanoholes in In0.52Al0.48As layers *AIP Adv.* **13** 055009
[26] Paul M, Olbrich F, Höschele J, Schreier S, Kettler J, Portalupi S L, Jetter M and Michler P 2017 Single-photon emission at 1.55 μm from MOVPE-grown InAs quantum dots on InGaAs/GaAs metamorphic buffers *Appl. Phys. Lett.* **11** 033102
[27] Miyazawa T *et al* 2016 Single-photon emission at 1.5 μm from an InAs/InP quantum dot with highly suppressed multi-photon emission probabilities *Appl. Phys. Lett.* **109** 132106
[28] Holewa P *et al* 2024 High-throughput quantum photonic devices emitting indistinguishable photons in the telecom C-band *Nat. Commun.* **15** 3358
[29] Hauser N *et al* 2026 Deterministic and highly indistinguishable single photons in the telecom C-band *Nat. Commun.* **17** 537
[30] Yang J *et al* 2024 High-rate intercity quantum key distribution with a semiconductor single-photon source *Light Sci. Appl.* **13** 150
[31] Chellu A, Hilska J, Penttinen J-P and Hakkarainen T 2021 Highly uniform GaSb quantum dots with indirect–direct bandgap crossover at telecom range *APL Mater.* **9** 051116
[32] Zhai L, Löbl M C, Nguyen G N, Ritzmann J, Javadi A, Spinnler C, Wieck A D, Ludwig A and Warburton R J 2020 Low-noise GaAs quantum dots for quantum photonics *Nat. Commun.* **11** 4745
[33] Keil R, Zopf M, Chen Y, Höfer B, Zhang J, Ding F and Schmidt O G 2017 Solid-state ensemble of highly entangled photon sources at rubidium atomic transitions *Nat. Commun.* **8** 15501
[34] Liu J *et al* 2019 A solid-state source of strongly entangled photon pairs with high brightness and indistinguishability *Nat. Nanotechnol.* **14** 586
[35] Huo Y H *et al* 2013 Ultra-small excitonic fine structure splitting in highly symmetric quantum dots on GaAs (001) substrate *Appl. Phys. Lett.* **102** 152105
[36] Huber D, Reindl M, Huo Y, Huang H, Wildmann J S, Schmidt O G, Rastelli A and Trotta R 2017 Highly indistinguishable and strongly entangled photons from symmetric GaAs quantum dots *Nat. Commun.* **8** 15506
[37] Schöll E 2019 Resonance fluorescence of GaAs quantum dots with near-unity photon indistinguishability *Nano Lett.* **19** 2404
[38] Huber D 2018 Strain-tunable GaAs quantum dot: a nearly dephasing-free source of entangled photon pairs on demand *Phys. Rev. Lett.* **121** 033902
[39] Michl J, Peniakov G, Pfenning A, Hilska J, Chellu A, Bader A, Guina M, Höfling S, Hakkarainen T and Huber-loyola T 2023 Strain-free GaSb quantum dots as single-photon sources in the telecom S-band *Adv. Quantum Technol.* **6** 2300180
[40] Huang S H, Balakrishnan G, Khoshakhlagh A, Jallipalli A, Dawson L R and Huffaker D L 2006 Strain relief by periodic misfit arrays for low defect density GaSb on GaAs *Appl. Phys. Lett.* **88** 131911
[41] Huang S H, Balakrishnan G, Khoshakhlagh A, Dawson L R and Huffaker D L 2008 Simultaneous interfacial misfit array formation and antiphase domain suppression on miscut silicon substrate *Appl. Phys. Lett.* **93** 071102

[42] Rodriguez J B, Madiomanana K, Cerutti L, Castellano A and Tournié E 2016 x-ray diffraction study of GaSb grown by molecular beam epitaxy on silicon substrates *J. Cryst. Growth* **439** 33
[43] Tournie E, Monge Bartolome L, Rio Calvo M, Loghmari Z, Díaz-thomas D A, Teissier R, Baranov A N, Cerutti L and Rodriguez J-B 2022 Mid-infrared III–V semiconductor lasers epitaxially grown on Si substrates *Light Sci. Appl.* **11** 165
[44] Leguay L, Chellu A, Hilska J, Luna E, Schliwa A, Guina M and Hakkarainen T 2024 Unveiling the electronic structure of GaSb/AlGaSb quantum dots emitting in the third telecom window *Mater. Quantum Technol.* **4** 015401
[45] Reindl M, Weber J H, Huber D, Schimpf C, Covre da Silva S F, Portalupi S L, Trotta R, Michler P and Rastelli A 2019 Highly indistinguishable single photons from incoherently excited quantum dots *Phys. Rev. B* **100** 155420
[46] Germanis S, Chen X, Dost R, Hallett D J, Clarke E, Patil P K, Skolnick M S, Wilson L R, Siampour H and Fox A M 2025 Waveguide excitation and spin pumping of chirally coupled quantum dots *Optica* **12** 1689–96
[47] Liu F, Martins L M P, Brash A J, Barth A M, Quilter J H, Axt V M, Skolnick M S and Fox A M 2016 Ultrafast depopulation of a quantum dot by LA-phonon-assisted stimulated emission *Phys. Rev. B* **93** 161407
[48] Thomas S E *et al* 2021 Bright polarized single-photon source based on a linear dipole *Phys. Rev. Lett.* **126** 233601
[49] Siampour H, O'rourke C, Brash A J, Makhonin M N, Dost R, Hallett D J, Clarke E, Patil P K, Skolnick M S and Fox A M 2023 Observation of large spontaneous emission rate enhancement of quantum dots in a broken-symmetry slow-light waveguide *npj Quantum Inf.* **9** 15
[50] Guina M, Rantamäki A and Härkönen A 2017 Optically pumped VECSELs: review of technology and progress *J. Phys. D: Appl. Phys.* **50** 383001
[51] Burd S C *et al* 2023 VECSEL systems for quantum information processing with trapped beryllium ions *J. Opt. Soc. Am. B* **40** 773–81
[52] Burd S C 2016 VECSEL systems for the generation and manipulation of trapped magnesium ions *Optica* **3** 1294–9
[53] Penttinen J-P *et al* 2024 Sub-Hz single-frequency VECSELs for optical clocks PC1291207
[54] Pooley M A 2012 Controlled-NOT gate operating with single photons *Appl. Phys. Lett.* **100** 211103
[55] Ferrini R, Galli M, Guizzetti G, Patrini M, Bosacchi A, Franchi S and Magnanini R 1997 Phonon response of AlxGa1−xSb/GaSb epitaxial layers by Fourier-transform infrared-reflectance and Raman spectroscopies *Phys. Rev. B* **56** 7549
[56] Hui L, Kai Z, Jingbiao P, Yundong S, Zhu W and Youwen Z 2011 Defect properties of as-grown and electron-irradiated Te-doped GaSb studied by positron annihilation *Semicond. Sci. Technol.* **26** 075016
[57] Kujala J, Segercrantz N, Tuomisto F and Slotte J 2014 Native point defects in GaSb *J. Appl. Phys.* **116** 143508
[58] Gawełczyk M *et al* 2017 Exciton lifetime and emission polarization dispersion in strongly in-plane asymmetric nanostructures *Phys. Rev. B* **96** 245425
[59] Gazzano O, Michaelis de Vasconcellos S, Arnold C, Nowak A, Galopin E, Sagnes I, Lanco L, Lemaître A and Senellart P 2013 Bright solid-state sources of indistinguishable single photons *Nat. Commun.* **4** 1425
[60] Graf A, Sonnenberg D, Paulava V, Schliwa A, Heyn C and Hansen W 2014 Excitonic states in GaAs quantum dots fabricated by local droplet etching *Phys. Rev. B* **89** 115314
[61] Rodt S, Heitz R, Schliwa A, Sellin R L, Guffarth F and Bimberg D 2003 Repulsive exciton-exciton interaction in quantum dots *Phys. Rev. B* **68** 035331
[62] Lettner T *et al* 2021 Strain-controlled quantum dot fine structure for entangled photon generation at 1550 nm *Nano Lett.* **21** 10501–6
[63] Chen C *et al* 2024 Wavelength-tunable high-fidelity entangled photon sources enabled by dual Stark effects *Nat. Commun.* **15** 5792
[64] Hopfmann C, Sharma N L, Nie W, Keil R, Ding F and Schmidt O G 2021 Heralded preparation of spin qubits in droplet-etched GaAs quantum dots using quasiresonant excitation *Phys. Rev. B* **104** 075301
[65] Schimpf C 2021 Entanglement-based quantum key distribution with a blinking-free quantum dot operated at a temperature up to 20 K *Adv. Photonics* **3** 065001
[66] Stobbe S, Johansen J, Kristensen P T, Hvam J M and Lodahl P 2009 Frequency dependence of the radiative decay rate of excitons in self-assembled quantum dots: experiment and theory *Phys. Rev. B* **80** 155307
[67] Covre Da Silva S F *et al* 2026 Low-density InGaAs/AlGaAs quantum dots in droplet-etched nanoholes *Nano Lett.* **26** 953–60
[68] Covre Da Silva S F C, Undeutsch G, Lehner B, Manna S, Krieger T M, Reindl M, Schimpf C, Trotta R and Rastelli A 2021 GaAs quantum dots grown by droplet etching epitaxy as quantum light sources *Appl. Phys. Lett.* **119** 120502